Towards an aero-servo-elastic simulation capability for high-performance fighter aircraft

O.J. Boelens, B.B. Prananta & B.I. Soemarwoto
National Aerospace Laboratory, NLR
Anthony Fokkerweg 2, 1059 CM
Amsterdam, The Netherlands

boelens@nlr.nl, prant@nlr.nl, soemarwt@nlr.nl

M.R. Allan, K.J. Badcock
University of Glasgow
Glasgow, G12 8QQ
United Kingdom

Mark.Allan@ansys.com, gnaa36@aero.gla.ac.uk

W. Fritz
European Aeronautic Defence and Space Company
Postfach 801160
D-81663, München

Willy.Fritz@eads.net

ABSTRACT

Manoeuvres of high-performance fighter aircraft occur frequently at extreme flow conditions characterised by vortical flow. The involved non-linear flow phenomena continue to be a subject of intense studies. Recent advances in computational methods offer an opportunity to assess flight dynamic properties of a manoeuvre accurately through an approach, where the non-linear fluid, flight and structural dynamics for flexible bodies are coupled in the non-linear equation of motion. As a first step towards such an approach, this paper describes a coupling between the one-degree-of-freedom equation of motion of a rigid body and the inviscid flow equations. Results of simulations of a free-to-roll delta wing configuration with moving elevons at high angle of attack, performed by the University of Glasgow, EADS-M and NLR, are presented to demonstrate the potential of the approach. In addition these results are compared with the results obtained using a coefficient-based aerodynamic model.

LIST OF SYMBOLS

a^+_{ref}	Reference speed of sound	T	Period
b^+_{ref}	Reference half-span	u^+_∞	Free-stream velocity
c^+_{ref}	Reference chord ($= l^+_{ref}$)	u_{red}	Reduced velocity

c_{ϕ}^{+}	Damping coefficient	x,y,z	Cartesian co-ordinates
C_l	Roll moment coefficient	α	Angle of attack
$C_{l_{\dot{\phi}}}$	Rolling moment damping derivative	β	Yaw angle
$C_{l_{\delta ele}}$	Elevon induced rolling moment derivative	γ	Specific heat ratio
I_{ϕ}^{+},	Rotational mass moment of inertia	δ , δ_{ele}	Elevon deflection
k	Reduced frequency	ϕ	Roll angle
k_{ϕ}^{+}	Stiffness coefficient	$\dot{\phi}$	Roll rate
l_{ref}^{+}	Reference length	Λ_{LE}	Leading edge sweep angle
L^{+}	Aerodynamic roll moment	μ	Mass ratio
m_{ref}^{+}	Reference mass (=mass of delta wing)	ρ_{∞}^{+}	Free-stream density
S_{ref}^{+}	Reference surface	τ	Non-dimensional time
t^{+}	Time	ω_{ref}^{+}	Reference circular frequency

1.0 INTRODUCTION

Fighter aircraft design has been pushed towards the expansion of flight envelopes into extreme conditions (high angles of attack) and aggressive manoeuvres with high angular rates, involving strongly non-linear aerodynamic phenomena. The enhanced tactical agility potentially increases air combat exchange ratio. However, severe stability and control problems can arise that increase the probability of departure from controlled flight.

Unfortunately, because of strong non-linear aerodynamic phenomena involved [1], it can happen that predictive methods are not able to reveal the onset and nature of the problems early in the design phase. Sometimes, a problem appears after a full-scale flight test has been conducted. Continuing the program without solving the problem would put severe restriction on the aircraft performance, while pilots in operational squadrons would strongly object to artificial manoeuvre limits. On the other hand, the cost incurred to fix the problem can be very high. To keep the budget overshoot under control, fixes tend to be *ad hoc*. The situation gets worse if fixes are applied without a sound basis of fundamental understanding of the physics concerned.

A recent example is the problem encountered in the flight test program of F/A-18E/F. During transonic

manoeuvres the aircraft experienced an uncommanded lateral motion known as wing drop. As a consequence, quoted from the literature [1], a significant amount of additional testing and engineering support was required to find a successful solution to the wing drop problem. The fixes consisted of modifications to the leading edge flap schedule and addition of a porous fairing at the wing fold location. As a result of the wing drop problem, a national program was initiated in the United States, including extensive experimental and computational studies of abrupt wing stall [2-4].

A more severe case is when a stability and control problem appears during the operational phase. Such a problem can lead to accidents with loss of aircraft and pilot. An example can be found in literature [5], describing the loss of an F-16 after an out-of-control roll behaviour at a high angle of attack.

One of the important factors contributing to such accidents is inadequate representation of physical non-linearities underlying the flight control system of the fighter aircraft. The dynamic characteristics of an aircraft depend on the aerodynamic properties and their variation with aircraft attitudes, as well as the inertial, geometric and flexibility properties of the aircraft. Traditionally, it is sufficient to consider these aspects in separate disciplines due to the assumption of weak interactions. For example, in aerodynamics, the aircraft is often assumed to be rigid, and steady flow analyses are conducted to obtain the aerodynamic forces, moments, and loads. In flight mechanics studies, the steady-state flow solutions are used to assess the stability and control properties of the aircraft. In aeroelasticity, it is common practise to analyse structural stability using simplified aerodynamic models without interaction with rigid-modes. While such a mono-disciplinary approach has proven to be effective for many applications, it is not generally applicable. Parts of the flight envelope of modern fighter aircraft call for a coupled approach, in particular because of the non-linear fluid dynamics involved.

For specific areas in the flight envelope, one should use a high-fidelity model for the assessment of flight dynamic properties. Such a model is governed by the non-linear fluid, flight and structural dynamics equations coupled in the non-linear equation of motion for flexible bodies. The resulting aero-servo-elastic model accounts for the non-linearities throughout the simulation. This model ensures accurate determination of departure boundaries, facilitates the development of best recovery strategies, and supports optimal flight control law design. This paper presents an initial development effort at NLR, EADS-M and the University of Glasgow towards such high-fidelity flight dynamic models.

2.0 APPROACHES IN FLIGHT DYNAMIC ASSESSMENT

The flight dynamics under consideration refers to the characteristics of departure susceptibility, departure motion, and possible recovery from departure. The characteristics depend on the aerodynamic properties and their variation with aircraft attitudes, as well as the inertial and geometric properties of the aircraft. Based on the physics modelled, three levels of flight dynamic assessment can be identified:

- **Level-1**. At this level, the assessment is based on the values and derivatives of the aerodynamic force and moment coefficients at representative steady conditions, which are obtained through a flight test, experimentally in a wind tunnel, or numerically using CFD. For example, the longitudinal characteristic is evaluated using the parameter C_{m_α} or, for aircraft featuring relaxed static stability, a minimum nose-down control parameter C_m^* [6]. The lateral-directional characteristics are commonly evaluated based on the criteria expressed in terms of the well-known parameter $C_{n_{\beta_{dyn}}}$, the Lateral Control Departure Parameter (LCDP) parameter, and the Synchronous Roll-Yaw Parameter [7,8]. These parameters can give first estimates of the departure boundaries. For aggressive manoeuvres, however, a level-1 assessment may become unacceptably inaccurate [9].
- **Level-2**. The assessment is based on simulations that use an aerodynamic model. This model is

basically a set of linear expansions of the equation of motion around a certain number of points covering (part of) the flight envelope. The aerodynamic data at these points are also obtained through a flight test, experimentally in a wind tunnel, or numerically using CFD, but much more extensively than for a level-1 assessment. A manoeuvre is defined in terms of a starting condition and a control input schedule for a certain period of time. The simulation provides the time responses of the aircraft. Departures can be identified as incipient temporal excursions in the angle of attack, yaw angle and rotational rates [9,10]. However, a level-2 approach is still limited, because the aerodynamic data can only be obtained for a limited number of points. When a prolonged excursion occurs, the simulation may enter a domain where no data is available and extrapolation is usually employed. Obviously, the validity of an extrapolated model is questionable.

- **Level-3**. At this level, the non-linear fluid, flight and structural dynamics are coupled in the non-linear equation of motion for flexible bodies. The resulting aero-servo-elasticity simulation capability, which accounts for the non-linearities throughout the simulation, ensures an accurate flight dynamic assessment. Another important advantage is that a level-3 assessment can be performed well into a domain where a flight test would incur too much safety hazards.

The paper pursues the high-fidelity option of level-3 assessments. Two influential aspects in such a capability are: (i) the capability of the CFD method to capture details of the flow physics, and (ii) the coupling of the flow equations and the equations of motion. Both these aspects are discussed in this paper. In addition results obtained by a level-2 method at the University of Glasgow will be discussed.

3.0 CFD-BASED SIMULATIONS TOWARDS A LEVEL-3 ASSESSMENT

3.1 Test case

The test case employs the 65° leading edge sweep WI1-SLE delta wing model including sting that belongs to a vortical flow computational and experimental program [11,12]. The planform definition of this delta wing is depicted in Figure 1. The aspects required for obtaining the high-fidelity capability for level-3 assessment are discussed by means of the following test case:

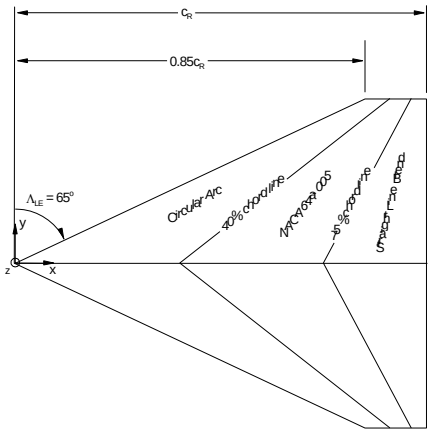

Figure 1: Planform definition of delta wing

– A free-to-roll delta wing configuration with moving elevons having non-dimensional inertial data

representative of a real fighter aircraft. The simulation is performed in an inviscid flow. The elevons are defined by $0.9 < x/c_{ref}^{+} < 1$ and $\pm 0.1 < y/b_{ref}^{+} < \pm 1$. The delta wing model is initially at an equilibrium position at zero roll-angle and an angle of attack of 17º, with the elevon deflection set to zero. A time schedule of elevon deflection is prescribed. The elevon deflection is realised by a continuous deformation of the wing surface. The model subsequently undergoes a one-degree-of-freedom oscillation due to the deflection of the elevons. During the simulation the following reference values have been used: $I_{\phi}^{+} = 0.37340 kgm^2$, $m_{ref}^{+} = 16.235 kg$, $\rho_{\infty}^{+} = 1.21 kg/m^3$, $a_{ref}^{+} = 340\, m/s$, $l_{ref}^{+} = 1m$ and $S_{ref}^{+} = 0.46 m^2$.

The roll-motion considered represents the attitude of an aircraft experiencing kinematic coupling, which is characterised by a conversion from high angle of attack to a large yaw angle. Such a kinematic coupling with adverse sideslip can lead to departure from controlled flight.

3.2 Level-2 coefficient-based aerodynamic model

At the University of Glasgow, a coefficient-based aerodynamic level-2 model for the rolling moment coefficient has been created based on a component build-up as described in standard textbooks, for example [13], given by

$$C_l = C_l(\alpha, \beta) + C_{l_{\dot{\phi}}} \dot{\phi} + C_{l_{\delta ele}}(\alpha, \beta)\delta_{ele}$$

The rolling moment data was found to be non-linear over the effective angle of attack and slide-slip angle range considered. Therefore, an aerodynamic database has been generated in order to estimate the various coefficients. The term $C_l(\alpha, \beta)$ is the baseline component that can be obtained by linearly interpolating between data from steady-state simulations for various angles of attack and yaw angles. The term $C_{l_{\dot{\phi}}}$ is the rolling moment damping derivative and was found to be constant over the range of roll rates considered. The term $C_{l_{\delta ele}}(\alpha, \beta)$ is the elevon induced rolling moment derivative. This term has also been obtained for any roll angle by linearly interpolating between data from steady-state simulations.

A simple routine has been written to evaluate the roll response of the WI1-SLE delta wing subject to the aerodynamic moment predicted by the above equation. The time integration was performed using a second-order accurate Runge-Kutta scheme. The results obtained using this level-2 model have been compared with the level-3 CFD-based results.

3.3 CFD Methods

The (Euler) flow equations are coupled with the equations of motion. As the presented test case involves only a rolling motion, a one-degree-of-freedom equation of motion is considered. Details on this coupling can be found in Appendix A.

3.3.1 University of Glasgow

At the University of Glasgow, the PMB (Parallel Multi-Block) RANS flow solver [14] has been used for the present simulation. This flow solver uses a cell-centred finite volume scheme to solve the Euler and Reynolds-Averaged Navier-Stokes equations. The diffusive terms are discretised using a central-differencing scheme, and the convective terms using Osher's approximate Riemann solver with MUSCL interpolation. Steady flow simulations proceed in two parts, initially running an explicit scheme, then switching to an implicit scheme to obtain quicker convergence. The linear system arising at each implicit step is solved using a Krylov subspace method. The preconditioning is based on a Block Incomplete

Lower-Upper BILU(0) factorisation, which is decoupled across blocks. For time-accurate simulations, Jameson's pseudo-time (dual-time stepping) formulation is applied, with the steady state solver used to calculate the flow steady states on each physical time step.

3.3.2 NLR

NLR's CFD system ENFLOW [15] has been applied to perform the simulations. The spatial discretisation of the flow solver employs a cell-centred finite volume scheme on multi-block structured grids. For time-dependent simulations, a second-order dual-time stepping scheme is applied, using a five-stage explicit Runge-Kutta scheme for each physical time step, with acceleration techniques such as local time stepping, implicit residual averaging and multi-grid.

3.3.3 EADS-M

At EADS-M the simulations have been performed using an in-house developed flow solver. This flow solver, which is used for pilot investigations in the coupling of aerodynamics and flight mechanics, works identical to FLOWer [16], but has a much simpler structure, i.e., only the Euler equations can be solved, only very simple block structures can be applied, and the code only runs on a single processor.

A cell-centred finite volume scheme is employed for the spatial discretisation. A second–order dual-time stepping scheme using a five-stage Runge-Kutta scheme is used for time-dependent simulations. Local time stepping, implicit residual smoothing and an explicit multi-grid scheme are employed to accelerate convergence. The numerical dissipation model is the anisotropic dissipation model as suggested by Jameson. In addition to this model, the dissipative flux vector has been optimised by a relaxation between the old and new values within the Runge-Kutta scheme.

The elevon deflection is incorporated by deforming the surface grid locally and subsequently regenerating the volume grid using a very fast hyperbolic grid generator, which is part of the flow solver.

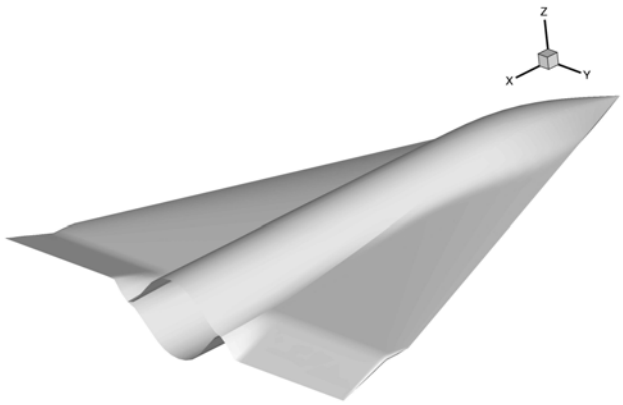

Figure 2: Convention for the positive asymmetric elevon deflection

4.0 RESULTS

The simulations have been performed on a C-O-type structured grid, having 72 points in the streamwise direction (49 points to the wing trailing edge), 129 points in the circumferential direction and 33 points in

the surface normal direction.

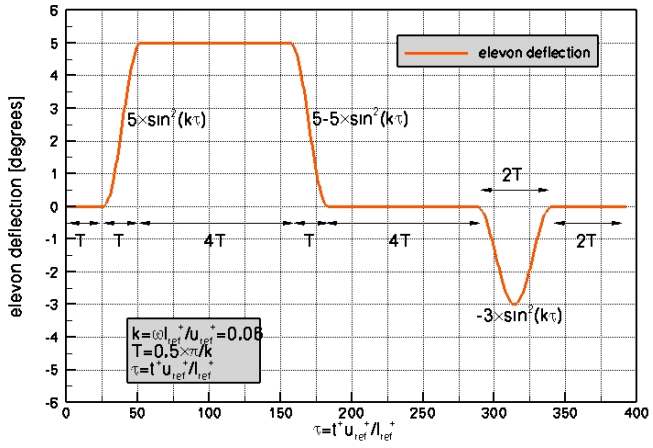

Figure 3: Schedule of the elevon deflection (M_∞=0.5, α=17°, inviscid flow)

The time schedule of elevon deflection used in the simulation is shown in Figure 3. A positive asymmetrical deflection means elevon down on the starboard side (pilot's view), see Figure 2. It should be noted that the convention of the roll motion and roll angle follows the convention of the elevon deflection.

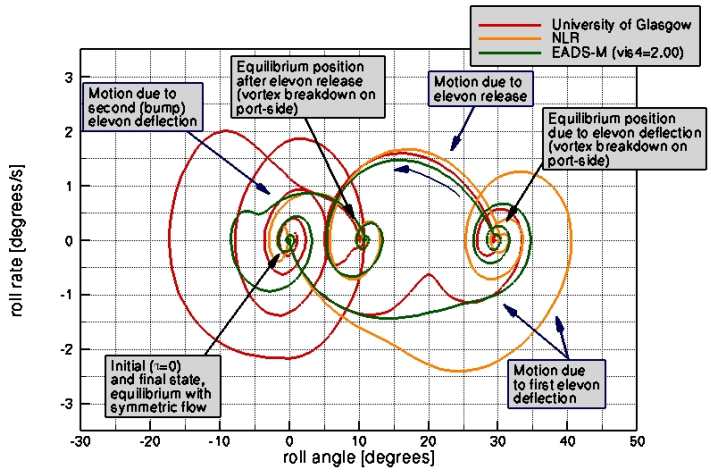

Figure 4: Variation of the roll rate and the roll angle during the simulation

In Figure 4 the variation of the roll rate and the roll angle during the simulation is shown. One way to analyse the motion of the delta wing is to consider the system as a classical second-order mass-spring-damper system, see also Appendix A. In the present case the stiffness coefficient k_ϕ^+ equals C_{l_ϕ} and the (viscous) damping coefficient c_ϕ^+ equals $C_{l_{\dot{\phi}}}$. Since for this case $C_{l_{\dot{\phi}}}$ is positive, the system is stable and allows for damped oscillatory motion around an equilibrium state. Experiments and simulations [12] have

shown that at an angle of attack of 17° the delta wing under consideration has three such equilibrium positions when the elevons are at their neutral position, i.e., zero degree roll angle, approximately 10° starboard side up roll angle and approximately 10° starboard side down roll angle. The former equilibrium position corresponds to a symmetric flow, whereas the latter two equilibrium positions are characterised by vortex breakdown on the portside and starboard side, respectively. In addition to these equilibrium positions, the elevon deflection results in other equilibrium positions for which the roll angle depends on the amplitude of the elevon deflection. For these positions the contribution to the roll moment induced by the elevon deflection is in balance with the contribution to the roll moment resulting from the leading edge vortices.

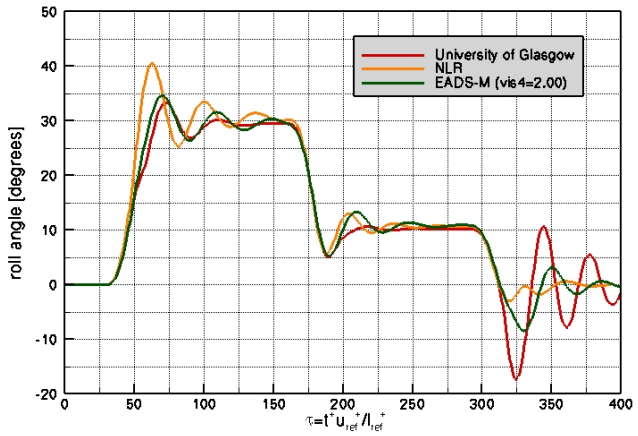

Figure 5: Response of the roll angle to the elevon deflection

Figure 5 and Figure 6 show the response of the roll angle and the roll-moment coefficient to the elevon deflection, respectively. Initially, the delta wing is at the zero-degree roll angle equilibrium position, characterised by symmetric flow and a zero roll-moment coefficient. Figure 7 shows the corresponding surface pressure coefficients. Both the University of Glasgow and NLR solution exhibit vortex breakdown. The position of the vortex breakdown is slightly more upstream for the University of Glasgow simulation.

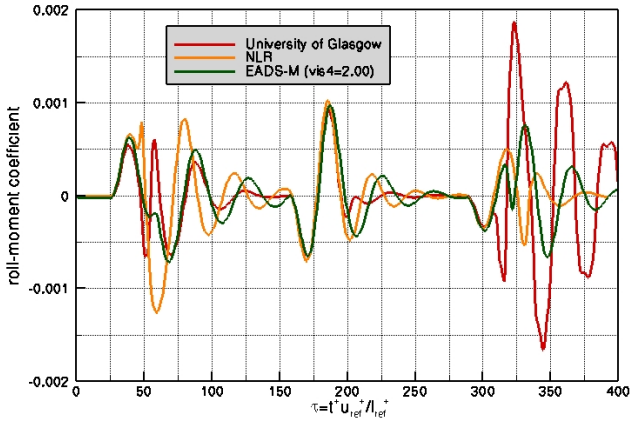

Figure 6: Response of the roll-moment coefficient to the elevon deflection

Starting at τ=26.9 the elevons are deflected from a zero degree elevon deflection to a maximum elevon deflection of 5° at τ=52.4. After τ=52.4 the elevon deflection is held constant at 5° until τ=157. When the elevon deflection is initially applied, the delta wing experiences a positive roll moment, and therefore rotates with the starboard side up (pilot's view). Due to this rotating motion the vortex structure above the delta wing will start to change. This rotating motion will give rise to an increase in yaw angle. The increase in yaw angle for the portside will result in vortex breakdown on this side of the delta wing, whereas the vortex on the starboard side will abstain from breakdown. This vortex structure will result in a negative roll moment on the delta wing. Eventually after several oscillations an equilibrium position will be reached for which both contributions to the roll moment, i.e., the one caused by the elevon deflection and the one caused by the vortex structure, are in balance. The final roll angle for all three simulations is approximately 30° starboard side up. The oscillation frequency is similar for all three simulations. However, the NLR simulation shows a more energetic less damped response than those observed for the University of Glasgow and EADS-M simulations, which are approximately similar. A reason for this might be that the NLR flow solver has less artificial dissipation (see also the discussion following Figure 12). In Figure 8 the surface pressure coefficient at τ=160 are presented. For all three simulations the pressure signature agrees with the above described vortex structure.

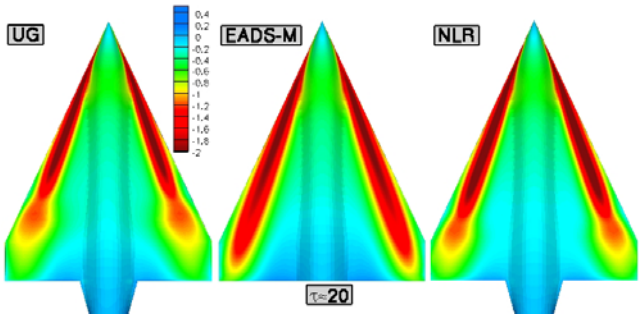

Figure 7: Surface pressure coefficient at the initial state, i.e., τ=20 (The sting is not shown in the EADS-M figure)

	UG	EADS-M	NLR
ϕ [°]	0.0	0.0	0.0

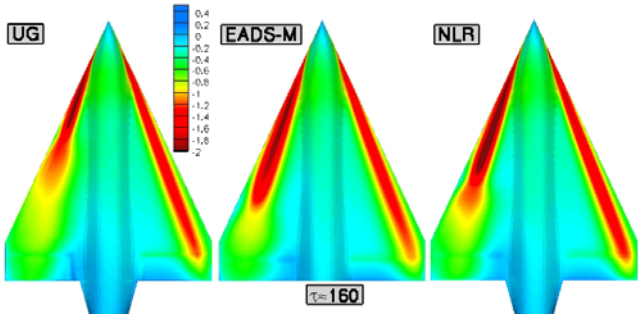

Figure 8: Surface pressure coefficient at the equilibrium position due to the elevon deflection (δ=5°), i.e., τ=160 (The sting is not shown in the EADS-M figure)

	UG	EADS-M	NLR
ϕ [°]	29.5	29.5	30.2

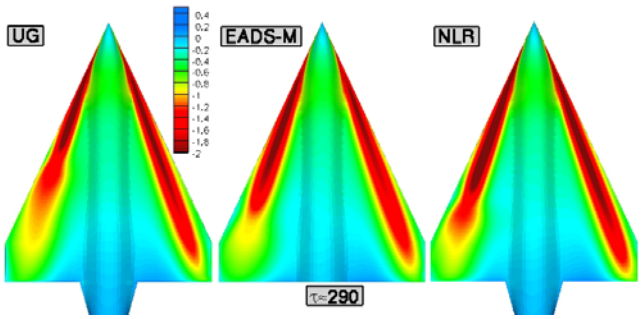

Figure 9: Surface pressure coefficient after the elevon release, i.e., τ=290 (The sting is not shown in the EADS-M figure)

	UG	EADS-M	NLR
ϕ [°]	10.2	10.9	10.7

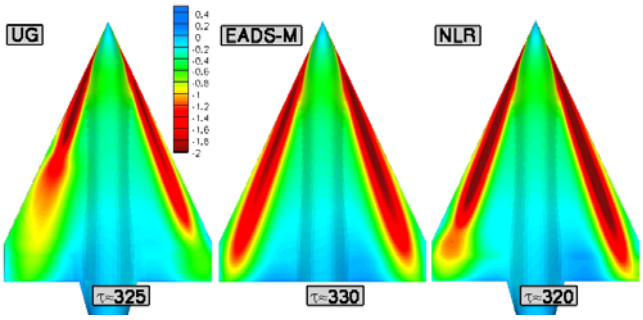

Figure 10: Surface pressure coefficient at the maximum roll angle after restoring elevon deflection (δ=-3°) (The sting is not shown in the EADS-M figure)

	UG	EADS-M	NLR
τ	325	330	320
ϕ [°]	-16.9	-8.4	-2.9

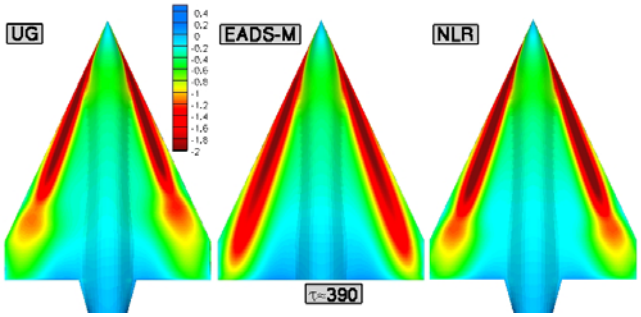

Figure 11: Surface pressure coefficient at the final state, i.e., τ=390 (The sting is not shown in the EADS-M figure)

	UG	EADS-M	NLR
ϕ [°]	2.9	0.5	0.0

Before the equilibrium position is reached, the elevon deflection is returned to zero degrees during the interval 157<τ<183. Next, the elevon deflection is held constant until τ=288. Since by removing the elevon deflection the roll moment caused by the elevons becomes zero, the delta wing starts, as a consequence of the still present negative roll moment due to the vortex structure, to rotate in the starboard side down direction. Instead of rotating towards the initial zero-degree roll angle equilibrium position, the delta wing halts after some oscillation at a roll angle of approximately 10° starboard side up. This roll angle corresponds with one of the previously observed equilibrium positions for this delta wing [12]. In Figure 9 the surface pressure coefficient at τ=290 is shown. All three simulations show similar signatures with vortex breakdown on the portside of the delta wing and a completely developed vortex on the starboard side of the delta wing.

Finally, a negative bump-like elevon deflection of 3° is applied during the interval 288<τ<340 which restores the attitude of the delta wing to the initial equilibrium position at zero degree roll angle. During this final part of the motion the oscillatory amplitude for the EADS-M simulation and especially for the University of Glasgow simulation is much larger than that for the NLR simulation. Note that the University of Glasgow simulation also passes the equilibrium position at approximately 10° starboard side down roll angle, but does not halt in this position. In Figure 10 the surface pressure coefficients at the maximum roll angle are shown. At this maximum roll angle the University of Glasgow simulation shows a pronounced vortex breakdown at the portside of the delta wing. The NLR simulation also shows vortex breakdown, however, at a much aft location, whereas in the EADS-M simulation both vortices are completely recovered. In Figure 11 the surface pressure coefficient at the final state, τ=390, is presented. Note that the roll angle corresponding to these figures has only reached the zero degree roll angle equilibrium position for the NLR simulation, while the other simulations still exhibit oscillatory behaviour. The agreement with the initial state shown in Figure 7 is, however, good.

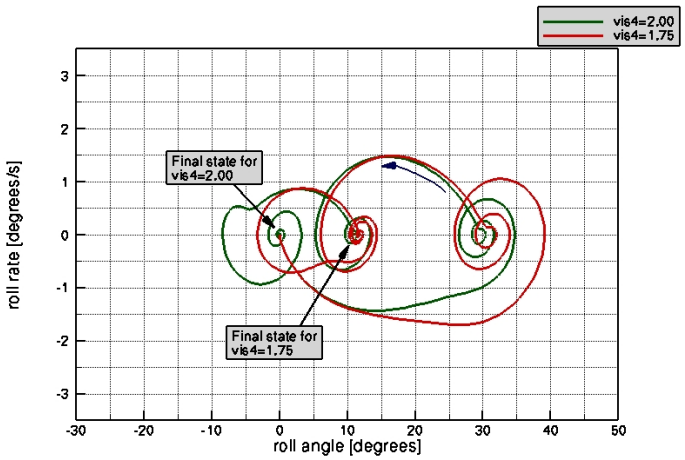

Figure 12: Variation of the roll rate and the roll angle for varying 4th order artificial dissipation coefficient (EADS simulation)

Figure 12 shows the variation of the roll rate and the roll angle for a varying 4th order artificial dissipation coefficient. These simulations have been performed by EADS-M. The 4th order artificial dissipation has been varied by varying the value of the vis4 coefficient, i.e., the constant coefficient multiplying the 4th order artificial dissipation, in the flow solver. A value of the vis4 coefficient equal to 2.00 has been used during the above-described simulation. In addition, a simulation has been performed for a lower value of the vis4 coefficient equal to 1.75. The initial part of the motion, i.e., until τ=288, is similar for both values of the coefficient. After the initial elevon deflection both simulations halt at the equilibrium position at approximately 30° starboard side up and subsequently after the release of the elevon deflection at the equilibrium position at approximately 10° starboard side up. Approaching the former equilibrium position the simulation using a lower dissipation coefficient, however, shows a more energetic less damped response, similar to the NLR simulation. After the negative bump-like elevon deflection both simulations follow different paths. As discussed before the higher artificial dissipation simulation follows a path that leads to the initial equilibrium position at zero degree roll angle. The lower artificial dissipation simulation on the other hand follows a path that leads back to the equilibrium position at a roll angle of approximately 10° starboard side up. These simulations show that the motion of the delta wing following the bump-like elevon deflection is very sensitive, as it depends to a large degree to the recovery of the burst portside vortex, that amongst others is affected by factors like the numerical dissipation and the shape of the elevon excitation.

The sensitivity to the elevon excitation is also shown by a simulation that has been performed by NLR in which a slightly larger negative bump-like elevon deflection (3.5° instead of 3°) has been applied, see Figure 13. For this elevon deflection the delta wing follows a path to the equilibrium position at a roll angle of approximately 10° starboard side down, for which vortex breakdown occurs at the starboard side of the wing.

Finally, in Figure 14 the variation of the roll rate and the roll angle for the CFD-based and the level-2 coefficient-based (see section 3.2) aerodynamic model are compared. These simulations have been performed at the University of Glasgow. During the first part of the simulation, i.e., $0<\tau<180$, the coefficient-based aerodynamic model shows a more energetic less damped response than the CFD-based model. The peak roll angle for the coefficient-based aerodynamic model is approximately 39° starboard side up, whereas the CFD simulation only reaches a roll angle of approximately 34° starboard side up. During the interval $180<\tau<290$, the CFD-based model follows a path towards the equilibrium position at a

roll angle of approximately 10° starboard side up. This non-zero roll angle equilibrium position, corresponding to an effective angle of attack of 16.75° and an effective yaw angle of 3°, is not found by the coefficient-based model. Investigating the $C_l(\alpha,\beta)$-curves underlying the coefficient-based model showed that in these curves such an equilibrium position is not present. Additional simulations, however, have shown that a static hysteresis is present that was not included in the coefficient-based model. Including such history effects that are associated with vortex breakdown would allow for the prediction of the non-zero roll angle equilibrium position by the coefficient-based model. For the final part of the motion, 290<τ<400, the CFD-based model and the coefficient-based aerodynamic model converge to the same final equilibrium position. During this interval the roll angle does not exceed a value of approximately 10° starboard side up corresponding to the equilibrium position, so that the above-mentioned hysteresis effects are not influencing the motion.

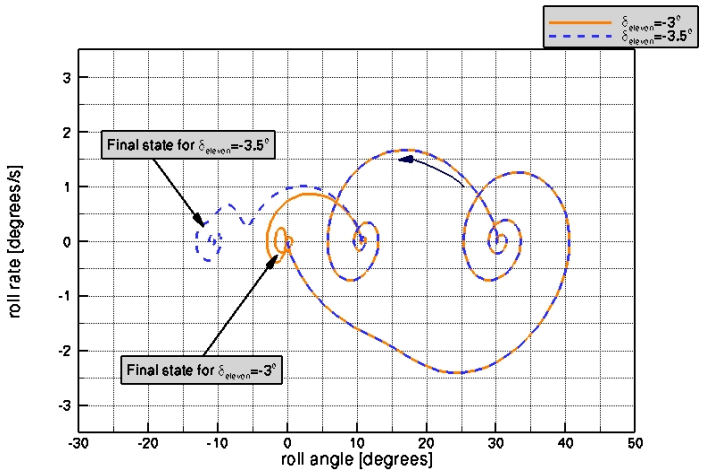

Figure 13: Variation of the roll rate and the roll angle for varying bump-like elevon deflection (NLR simulation)

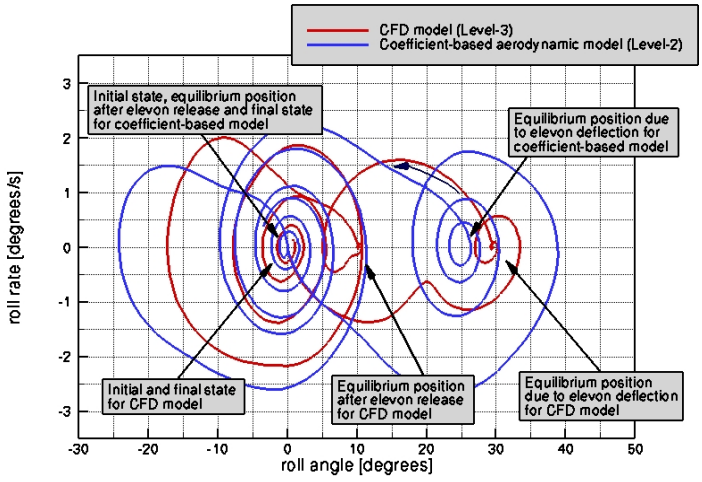

Figure 14: Variation of the roll rate and the roll angle for CFD-based and Level-2 coefficient-based aerodynamic model (University of Glasgow simulation)

5.0 CONCLUSIONS

An initial development effort towards obtaining a level-3 capability for flight dynamic assessment has been presented. Such a level-3 capability is governed by the non-linear fluid, flight and structural dynamics equations coupled in the non-linear equation of motion for flexible bodies. Simulation results for both this level-3 method and a coefficient-based level-2 method developed by the University of Glasgow have been shown for a 65° leading edge sweep delta wing configuration at a high angle of attack experiencing free-to-roll motion due to a scheduled control elevon input. Although the effort described is still initial in nature, e.g., since only one-degree-of-freedom motion is considered and no feedback such as that from an automatic control is modelled, the test case contains some essential elements of realistic strongly non-linear high-angle-of-attack aerodynamics, that determine the outcome of a manoeuvre.

The test case has shown that, although the different flow solvers of NLR, EADS-M and the University of Glasgow predict different vortex structures, e.g., with respect to vortex strength and breakdown location, the resulting motion and equilibrium positions are in good agreement. This means that the equilibrium positions and the paths towards those are mainly determined by the difference in vortex strength between the portside and the starboard side of the wing. Modifying factors like the numerical dissipation and the shape of the elevon excitation can, however, by influencing this difference, alter the equilibrium positions and paths towards those positions.

Comparison between the results obtained using the level-2 coefficient-based method and the level-3 method has shown that for the prediction of non-linear effects by coefficient-based methods, such as the non-zero roll angle equilibrium positions, history effects need to be included in such a method. This is of importance for all flight mechanics modelling where in general hysteresis effects are present.

The next step will be to apply the capability to multi-degree-of-freedom motion for a realistic fighter aircraft configuration. Subsequently structural flexibility effects, i.e., aeroelastic deformation, will be included. The main challenges in future research will be to incorporate a complete model of pilot input, to include control laws, and to perform simulations near the edges of the flight envelope. The assessment can then lead to an accurate determination of departure boundaries, facilitate the development of best recovery strategies, and support optimal flight control law design.

6.0 ACKNOWLEDGEMENTS

The test case reported in this paper has been studied in the framework of THALES JP12.15, which is a collaborative research between Alenia, DLR, EADS, NLR, QinetiQ and the University of Glasgow, performed under the auspices of the Western European Armaments Group (WEAG). The work has been conducted within the THALES JP12.15 contract granted by the Ministries of Defence of the representative nations.

7.0 REFERENCES

[1] Nelson, R.C., Alain, P., ‘The unsteady aerodynamics of slender wings and aircraft undergoing large amplitude maneuvers’, *Progress in Aerospace Sciences* 39 (2003) 185-248.

[2] Cook, S., Chambers, J., Kokolios, A., Niewoehner, R., Owens, D., Roesch, M., ‘An integrated approach to assessment of abrupt wing stall for advanced aircraft’, *AIAA Paper 2003-0926*, 2003.

[3] McMillin, N., Hall, R., Lamar, J., ‘Transonic Experimental Observations of abrupt wing stall on an F/A-18E Model’, *AIAA Paper 2003-0591*, 2003.

[4] Woodson, S., Green, B., Chung, J., Grove, D., Parikh, P., Forsythe, J., ‘Understanding abrupt wing

stall with CFD', *AIAA Paper 2003-0592*, 2003.

[5] Anderson, S.B., 'Handling qualities related to stall/spin accidents of supersonic fighter aircraft', *J. Aircraft*, vol. 22, no. 10, pp. 875-880, 1985.

[6] Nguyen, L.T., Foster, J.V., 'Development of a preliminary high-angle-of-attack nose-down pitch control requirement for high-performance aircraft ', *NASA TM-101684*, 1990.

[7] Weismann, R., 'Preliminary criteria for predicting departure characteristics/spin susceptibility of fighter-type aircraft', *J. of aircraft*, vol. 10, no.4, pp. 214-219, 1973.

[8] Charlton, E.F., 'Numerical Stability and Control Analysis Towards Falling Leaf Prediction Capabilities of Splitflow for Two Generic High-Performance Aircraft Models', *NASA CR-1998-208730*, 1998.

[9] Bihrle Jr., W., Barnhart, B., 'Departure susceptibility and uncoordinated roll-reversal boundaries for fighter configurations', J. of Aircraft, vol. 19, no. 11, pp. 897-903, 1982.

[10] Ryan III, G.W., 'A genetic search technique for identification of aircraft departures', *NASA CR-4688*, 1995.

[11] Soemarwoto, B.I., Boelens, O.J., Allan, M., Arthur, M.T., Bütefisch, K., Ceresola, N., Fritz W., 'Towards the simulation of unsteady manoeuvre dominated by vortical flow', *AIAA Paper 2003-3528*, 2003.

[12] Arthur, M.T., Allan, M., Ceresola, N., Kompenhans, J., Fritz, W., Boelens, O.J., Prananta, B.B., 'Exploration of the Free Rolling Motion of a Delta Wing Configuration in Vortical Flow', RTO-MP-AVT-123 Paper 1, Budapest, 2005.

[13] Stevens, B.L. and Lewis, F.L., 'Aircraft simulation and control', ISBD 0-471-61397-5, John Wiley and Sons Inc., 1992.

[14] Badcock, K.J., Richards, B.E., and Woodgate, M.A., 'Elements of Computational Fluid Dynamics on block structured grids using implicit solvers', Progress in Aerospace Sciences, Vol. 36, pp 351-392, 2000.

[15] Boerstoel, J.W., Kassies, A., Kok, J.C., and Spekreijse, S.P., 'ENFLOW, A full-functionality system of CFD codes for industrial Euler/Navier-Stokes Flow Computations', *NLR TP 96286*, 1996.

[16] Aumann, P., Bartelheimer, W., Bleecke, H., Eisfeld, J., Lieser, J., Heinrich, R., Kroll, N., Kuntz, M., Monsen, E., Raddatz, J., Reisch, U., and Roll, B., 'FLOWer Installation and USER Handbook Release 116', DLR Document MEGAFLOW-1001, 2000.

APPENDIX A

The equation governing one-degree-of-freedom rolling motion is coupled with the flow equations within the representative flow solvers. This equation of motion reads

$$I_\phi^+ \frac{d^2\phi}{dt^{+2}} + c_\phi^+ f\left(\frac{d\phi}{dt^+}\right) + k_\phi^+ \phi = L^+$$

where I_ϕ^+ is the rotational mass moment of inertia, c_ϕ^+ is the damping coefficient and k_ϕ^+ the stiffness coefficient. In this equation, the superscript $+$ denotes variables with physical dimensions. This equation is representative for a classical second-order mass-spring-damper system.

For the present test case, the delta wing moves freely. Therefore, there is no mechanical damping , i.e., $f\left(\frac{d\phi}{dt^+}\right) = 0$, and $k_\phi^+ = 0$. Furthermore, this means that the only damping acting on the motion enters implicitly into the equation of motion through the aerodynamic roll moment L^+.

NLR solution procedure

After scaling the above equation with the proper reference parameters and including that the delta wing moves freely, the non-dimensional equation of rolling motion is obtained, i.e.,

$$\frac{d^2\phi}{d\tau^2} = \frac{U_{red}^2}{2\mu I_\phi} C_l$$

with $I_\phi = \frac{I_\phi^+}{m_{ref}^+ l_{ref}^{+2}}$, $C_l = \frac{L^+}{\frac{1}{2}\rho_\infty^+ u_\infty^{+2} l_{ref}^{+3}}$ and $\omega_{ref}^+ = \frac{1}{t_{ref}^+}$.

The non-dimensional parameters governing the coupling between the flow equations and the equation of rigid body motion are the so-called reduced velocity $U_{red} = \frac{u_\infty^+}{\omega_{ref}^+ l_{ref}^+}$ and the mass ratio $\mu = \frac{m_{ref}^+}{\rho_\infty^+ l_{ref}^{+3}}$. The integration of the equation of motion in time is carried out using the transfer matrix method, i.e.,

$$\bar{\Phi}^{n+1} = e^{A\Delta t}\bar{\Phi}^n + \int_n^{n+1} e^{A\Delta t} B C_l(\tau, \phi) d\tau ,$$

where

$$\bar{\Phi} = \begin{pmatrix} \phi \\ d\phi/dt \end{pmatrix}, A = \begin{bmatrix} 0 & 1 \\ 0 & 0 \end{bmatrix}, B = \frac{U_{red}^2}{2\mu}\begin{pmatrix} 0 \\ -I_\phi^{-1} \end{pmatrix}.$$

University of Glasgow solution procedure

At the University of Glasgow, the non-dimensional equation of rolling motion is redefined as

$$\frac{d^2\phi}{d\tau^2} = \frac{\rho_\infty^+ l_{ref}^{+5}}{I_\phi^+} C_l$$

with $C_l = \dfrac{L^+}{\rho_\infty^+ u_\infty^{+2} l_{ref}^{+3}}$.

This equation has been coupled to the PMB RANS flow solver by evaluating the flight mechanics equation in the pseudo-time loop of the dual-time stepping scheme. In this way, the flight mechanics equation converges with the flow solution minimising sequencing errors. The most recent update for the rolling moment coefficient C_l is used in the evaluation of the roll angle and roll rate at the following pseudo-time step. The implicit time integration scheme is given by

$$\vec{q}^{\,n+1,k} = \vec{q}^{\,n} + \frac{\Delta\tau}{2}\left(\vec{R}^{\,n+1,k} + \vec{R}^{\,n}\right) \text{ where } \vec{q} = \begin{pmatrix} \phi \\ d\phi/d\tau \end{pmatrix} \text{ and } \vec{R} = \begin{pmatrix} d\phi/d\tau \\ \rho_\infty^+ l_{ref}^{+5} \Big/ I_\phi^+ \, C_l \end{pmatrix}.$$

EADS-M solution procedure

At EADS-M, the non-dimensional equation of rolling motion is rewritten as

$$\frac{d^2\phi}{d\tau^2} = \frac{\gamma M_\infty^2}{\mu R_\phi^2} C_l$$

with γ the heat capacity ratio, R_φ the radius of inertia defined as $R_\phi = \sqrt{\dfrac{I_\phi^+}{m_{ref}^+ l_{ref}^{+2}}}$, $\tau = \dfrac{t^+ a_\infty^+}{\mathcal{M}_{ref}^+}$ the non-dimensional time, μ the mass ratio defined by $\mu = \dfrac{2m_{ref}^+}{\rho_\infty^+ S^+ l_{ref}^+}$ and $C_l = \dfrac{L^+}{\frac{1}{2}\rho_\infty^+ u_\infty^{+2} S_{ref}^+ l_{ref}^+}$. Here S_{ref}^+ is the reference surface.

This equation is integrated using a second-order accurate time integration scheme, which is included in the pseudo-time loop of the dual time stepping scheme.